Variational Estimation of the Wind Stress Drag Coefficient and the Oceanic Eddy Viscosity Profile

LISAN YU AND JAMES J. O'BRIEN

The Mesoscale Air–Sea Interaction Group, Florida State University, Tallahassee, Florida

ABSTRACT

A variational optimal control technique is used to assimilate both meteorological and oceanographic observations into an oceanic Ekman layer model. An identical twin experiment is discussed first in which the "observations" are created by the dynamic model. The field measurements from the LOTUS-3 (Long-Term Upper Ocean Study-3) buoy are then analyzed. By fitting the model results to the data, the unknown boundary condition (the wind stress drag coefficient) and the unknown vertical eddy viscosity distribution are deduced simultaneously from the data, and an optimal estimate of the current field is obtained.

Though the model is simple, the results show that the variational assimilation technique is capable of extracting from the available observations a reasonable wind stress drag coefficient and vertical eddy viscosity distribution.

1. Introduction

The wind-driven upper layer of the ocean plays an important role in the general oceanic circulation. Unfortunately, our knowledge of the surface forcing and mixing processes within this layer is far from complete, and we are forced to rely on relatively simple parameterizations of those processes. For example, the surface wind stress is often characterized by a surface drag coefficient, while turbulent mixing is defined by an eddy viscosity coefficient. In this paper, we demonstrate a method for obtaining optimal estimates of the surface drag coefficient and of the vertical distribution of eddy viscosity from observations of wind velocity and current velocity profiles within the water column. The results of such analyses should provide information useful for improving the turbulent mixing parameterizations in numerical ocean models.

The method uses variational optimal control techniques in combination with a modified Ekman layer model to simultaneously deduce the surface wind drag coefficient and the eddy viscosity distribution from observed data. The variational optimal control technique has been widely studied in meteorology and oceanography since its introduction by Sasaki (1970). The works by Derber (1985), Le Dimet and Talagrand (1986), Talagrand and Courtier (1987), Thacker and Long (1988), Wunsch (1987, 1988), Long and Thacker (1989), and Sheinbaum and Anderson

(1990), among others, have illustrated the feasibility and potential usefulness of the variational method.

The basic idea of the variational optimal control method is to define a cost function that quantifies the discrepancy between the model results and the observations; at its simplest, the cost function might be the sum of squared differences between observations and their model equivalents. The cost function is then minimized by varying the control parameters of the problem, e.g., the drag and eddy viscosity coefficients in the present application, while treating the dynamical model as a strong constraint (Sasaki 1970). A systematic approach for solving problems of this type is to define an augmented Lagrange function by using undetermined Lagrange multipliers to enforce the model constraints. The introduction of Lagrange multipliers leads to a new set of equations, the adjoint equations, that govern the multipliers. The adjoint equations effectively transform the model–data misfit into the gradient of the cost function with respect to the control parameters. The gradient can then be used within an appropriate iterative descent method to search out the optimal estimates of the control parameters.

In principal, the initial model state and all the parameters of the model dynamics can be determined by the variational method if sufficient data are given. Unfortunately, ocean observations are sparse and noisy. Therefore, theoretical knowledge is required to analyze and process the model results (Thacker 1988). For example, prior knowledge is used by Sheinbaum and Anderson (1990) to choose a good first-guess initial state not only to make the algorithm efficient, but also to have a realistic representation of what the field may be like in areas not constrained by the data. In our

---

Corresponding author address: Dr. Lisan Yu, Mesoscale Air–Sea Interaction Group, Mail Stop B-174, Love 012, Florida State University, Tallahassee, FL 32306-3041.

case, however, essentially continuous time series data are available at each grid point, so that at any given time the model control parameters can be completely resolved and the final results do not depend on the initial guess.

The plan of this paper is as follows. The methodology is given in section 2, including the description of the modified Ekman model, the problem of scaling, the formation of variational formalism, and the numerical scheme. In section 3, an identical twin experiment is performed first by using the variational algorithm. The observed meteorological and oceanographic fields are analyzed and discussed in section 4. The data used are taken from the LOTUS-3 (Long-Term Upper Ocean-Study-3) records. A summary of the results and a discussion are given in section 5.

2. Problem specification

a. Model description and the problem of scaling

Consider a continuously stratified and horizontally unbounded ocean surface layer with depth H. Take the z-axis vertically upwards, with $z = 0$ at the surface. The ocean is rotating about the z-axis, and the Coriolis parameter, f, is taken to be constant. Neglecting the changes of the ocean surface, the modified Ekman model is

$$\frac{\partial w}{\partial t} + ifw = \frac{\partial}{\partial z}\left(A\frac{\partial w}{\partial z}\right) \qquad (1.1)$$

where horizontal velocity components u and v (u positive to the east, v positive to the north) are combined into one complex vector $w = u + iv$; the eddy viscosity $A(z)$, which is the parameter to be calculated, is a function of depth.

This upper ocean satisfies the following boundary conditions. At the surface, the forcing is given by the wind stress $\tau = \tau^x + i\tau^y$ (τ^x in the x-direction, τ^y in the y-direction), i.e.,

$$\rho_w A\frac{\partial w}{\partial z} = \tau \quad \text{at} \quad z = 0 \qquad (1.2)$$

where ρ_w is the density of water.

The wind stress is calculated from $\tau = \rho_a c_D |w_a| w_a$ where ρ_a is the density of air; w_a is the complex vector of wind speed; and c_D is the drag coefficient and the other parameter to be determined.

At some depth H, the condition of no momentum flux is assumed, i.e.,

$$A\frac{\partial w}{\partial z} = 0 \quad \text{at} \quad z = -H. \qquad (1.3)$$

The initial condition for this dynamic system is

$$w = w_0 \quad \text{at} \quad t = 0. \qquad (1.4)$$

As mentioned above, we are going to estimate two kinds of parameters. One is the drag coefficient, which

enters in the upper boundary condition in the dynamic model. The other one is the eddy viscosity profile, which represents a physical property of the flow and varies with depth. Because of the physical nature of these parameters, it is clear that the variables have different units and magnitudes. The scaling issue thus arises (see Gill et al. 1981; Luenberger 1984). The basic rule of variable scaling is to make all the variables in the scaled problem of order unity, so that each variable has a similar "weight" during the optimization.

Since the motions in the upper ocean are dominated by the inertial oscillations, the inertial period $O(f^{-1})$ is chosen as the time scale. We introduce the following nondimensional variables into Eqs. (1.1)–(1.4):

$$t' = \frac{t}{T_f}, \quad w' = \frac{w}{U}, \quad z' = \frac{z}{D},$$

$$A' = \frac{A}{s_a}, \quad c_D' = \frac{c_D}{s_c}, \quad w_a' = \frac{w_a}{U_a}$$

where

$$T_f = \frac{1}{f}, \quad D = \left(\frac{s_a}{f}\right)^{1/2}, \quad \text{and} \quad U = \left(\frac{\rho_a}{\rho_w}s_c\right)\frac{U_a^2}{\sqrt{s_a f}}.$$

Hence, the nondimensional problem takes the form (after dropping all primes)

$$\frac{\partial w}{\partial t} + iw = \frac{\partial}{\partial z}\left(A\frac{\partial w}{\partial z}\right) \qquad (2.1)$$

with

$$A\frac{\partial w}{\partial z} = c_D|w_a|w_a \quad \text{at} \quad z = 0 \qquad (2.2)$$

$$A\frac{\partial w}{\partial z} = 0 \quad \text{at} \quad z = -\frac{H}{D} \qquad (2.3)$$

and

$$w = w_0 \quad \text{at} \quad t = 0. \qquad (2.4)$$

b. Variational analysis

In variational analysis, the solution of the problem is sought by minimizing the cost function, which measures the misfit between the model results and the data, while the model equations serve as the constraints. Considering the linear dynamics of our model, we choose a least squares fitting for the cost function. The cost function is then defined as

$$J(w, A, c_D) = \frac{1}{2}K_m \int_t \int_z (w - \hat{w})^2 d\zeta d\tau$$

$$+ \frac{1}{2}K_a T \int_z (A - \hat{A})^2 d\zeta + \frac{1}{2}K_c TH(c_D - \hat{c}_D)^2 \qquad (3)$$

where the carat denotes the observations or estimates. The coefficients K_m, K_a, and K_c are the Gauss precision moduli controlling the best fits for each type of data (Panchang and O'Brien 1988). The nondimensional

parameters T and H represent the total integration time and depth in the model.

The cost function (3) is composed of three terms. The first one is called the data misfit, which is the squared difference between the model solution and the observations. The last two terms measure the closeness of the estimated parameters between two iterations of the descent algorithm. Since parameter estimation is our main interest in this paper, the added terms represent prior information about the parameters that increase the chance that the cost function will be convex and therefore lead to a unique solution (Carrera and Neuman 1986; Smedstad 1989). The model solution resulting from minimizing the cost function will best agree with the observed data. The new estimates of the parameters will not deviate far from the values taken by the parameters at the previous iteration. In this sense, the parameters' initial guess should be as reasonable as possible so that the optimization process can perform efficiently.

The dynamic model equations, which are treated as the strong constraints, can be enforced by introducing a set of undetermined Lagrange multipliers. This leads to the formation of the augmented Lagrange function, given as

$$L(w, A, c_D, \lambda)$$

$$= J + \int_t \int_z \left\{ \lambda, \left(\frac{\partial w}{\partial t} + iw - \frac{\partial}{\partial z} \left(A \frac{\partial w}{\partial z} \right) \right) \right\} d\zeta d\tau \quad (4)$$

where $\{ \quad , \quad \}$ is the inner product of two vectors and $\lambda = \lambda_u + i\lambda_v$ is the complex vector of the Lagrange multipliers (λ_u for the u-component model equation, λ_v for the v-component). The boundary conditions do not appear as a constraint with their own Lagrange multipliers because they enter into the model equation through the forcing term in the finite-difference formalism. The constrained optimization problem is now replaced by a series of unconstrained problems with respect to the variables w, A, c_D and λ. By doing so, the problem of minimizing the cost function subject to the model equations becomes a problem of finding the stationary points of the augmented Lagrange function. This is equivalent to the determination of w, A, c_D, and λ under the condition that the gradient of the augmented Lagrange function vanishes, which yields the following set of equations:

$$\frac{\partial L(w, A, c_D, \lambda)}{\partial \lambda} = 0 \quad (5)$$

$$\frac{\partial L(w, A, c_D, \lambda)}{\partial w} = 0 \quad (6)$$

$$\frac{\partial L(w, A, c_D, \lambda)}{\partial A} = 0 \quad (7)$$

$$\frac{\partial L(w, A, c_D, \lambda)}{\partial c_D} = 0. \quad (8)$$

Equation (5) recovers the original model equation, while Eq. (6) results in the adjoint equation, given by

$$\frac{\partial \lambda}{\partial t} + i\lambda + \frac{\partial}{\partial z} \left(A \frac{\partial \lambda}{\partial z} \right) = K_m (w - \hat{w}). \quad (9)$$

Note that the following natural boundary and initial conditions have been used when deriving the adjoint equation: the net flux of the adjoint variable λ is required to be zero both at the top and at the bottom of the chosen computational domain, i.e.,

$$\frac{\partial \lambda}{\partial z} = 0 \quad \text{at} \quad z = 0 \quad \text{and} \quad z = -\frac{H}{D}$$

and the initial condition is

$$\lambda = 0 \quad \text{at} \quad t = T.$$

It is worth noting that the adjoint equation has a similar form to the original model equation, except for two important features. The friction term in the adjoint equation has the opposite sign to that in the model equation. The stability of the well-posed problem thus requires the integration of the adjoint equation to be backward in time. In addition, the driving factor for the adjoint equation is the square root of the data misfit. The Lagrange multipliers carry the information about the data back to the initial time to influence the reconstruction of the model state.

Using Eqs. (7) and (8), the gradient of the augmented Lagrange function L with respect to A and c_D yields

$$\frac{\partial J}{\partial c_D} = -\int_t (|w_a| u_a \lambda_{uz=0} + |w_a| v_a \lambda_{vz=0}) d\tau \quad (10)$$

$$\frac{\partial J}{\partial A} = -\int_t \left(\frac{\partial u}{\partial z} \frac{\partial \lambda_u}{\partial z} + \frac{\partial v}{\partial z} \frac{\partial \lambda_v}{\partial z} \right) d\tau \quad (11)$$

with Eq. (3), we can write:

$$c_D = \hat{c}_D - \frac{1}{K_c TH} \frac{\partial J}{\partial c_D}$$

$$= \hat{c}_D + \frac{1}{K_c TH} \int_t (|w_a| u_a \lambda_{uz=0} + |w_a| v_a \lambda_{vz=0}) d\tau \quad (12)$$

$$A = \hat{A} - \frac{1}{K_a T} \frac{\partial J}{\partial A}$$

$$= \hat{A} + \frac{1}{K_a T} \int_t \left(\frac{\partial u}{\partial z} \frac{\partial \lambda_u}{\partial z} + \frac{\partial v}{\partial z} \frac{\partial \lambda_v}{\partial z} \right) d\tau. \quad (13)$$

Equations (12)–(13) are for the control parameters, from which A and c_D can be determined by minimizing the cost function by the descent method. If we define

$\lambda/K_m = \lambda'$, $K_c/K_m = K_c'$ and $K_a/K_m = K_a'$, the three Gauss precision moduli K_c, K_a and K_m are replaced by K_c' and K_a'. In general, if one has n precision moduli, the number can be reduced to $n - 1$ by scaling. Then Eqs. (9), (12) and (13) are simplified to (dropping all the primes):

$$\frac{\partial\lambda}{\partial t} + i\lambda + \frac{\partial}{\partial z}\left(A\frac{\partial\lambda}{\partial z}\right) = (w - \hat{w}) \qquad (14)$$

$$c_D = \hat{c}_D + \frac{1}{K_c TH}\int_t (|w_a|u_a\lambda_{uz=0} + |w_a|v_a\lambda_{vz=0})d\tau \qquad (15)$$

$$A = \hat{A} + \frac{1}{K_a T}\int_t \left(\frac{\partial u}{\partial z}\frac{\partial\lambda_u}{\partial z} + \frac{\partial v}{\partial z}\frac{\partial\lambda_v}{\partial z}\right)d\tau. \qquad (16)$$

There are six unknowns, $u(z, t)$, $v(z, t)$, $A(z)$, c_D, $\lambda_u(z, t)$ and $\lambda_v(z, t)$, and six equations, (2), (14), (15), and (16); the system is closed. The parameters $\hat{A}(z)$, $\hat{c}_D$, T, H, K_a and K_c must be specified. The numerical scheme will be described in the following subsection.

c. Numerical method

The numerical model is formulated using a finite difference discretization on a grid with spatial increment Δz and temporal increment Δt. Its vertical structure is schematically shown in Fig. 1. The w points are staggered in space with the A points. The Crank–Nicholson scheme is employed (O'Brien 1986).

Our procedure for solving this system is

1) begin with a best initial estimate for the control parameters A and c_D;
2) integrate the model Eq. (2) forward in time and calculate the value of the cost function by using Eq. (3);
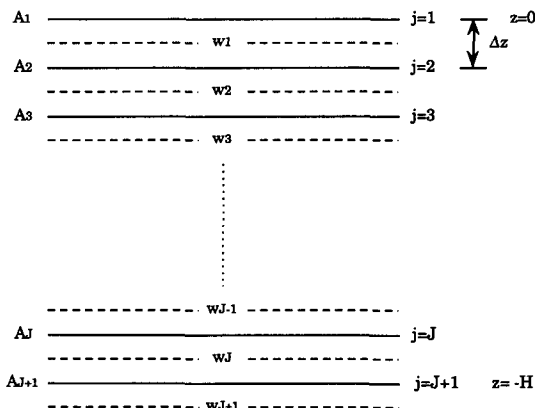3) compute the data misfits $(w - \hat{w})$;
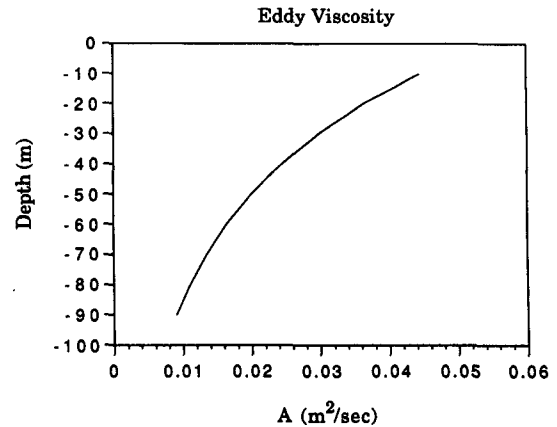

FIG. 2. The eddy viscosity profile used to create the "observations."

4) integrate the adjoint Eq. (14) backward in time;
5) use Eqs. (10) and (11) to calculate the components of ∇J (the gradients of the cost function) corresponding to c_D and A with solutions for λ and w from steps 2) and 4);
6) with the gradient information, apply the unconstrained minimization descent algorithm to obtain the new values of A and c_D simultaneously;
7) check if the convergence criterion

$$|\nabla J|/|\nabla J_0| < 10^{-2}$$

for the minimization process is satisfied, where ∇J_0 is the value at the initial iteration; and
8) return to step 2) if the optimal solution is not found.

This minimization determines the best fit of the data when the optimal solution is approached. Many different minimization methods are available (Navon and Legler 1987). The method we used is the limited-memory quasi-Newton conjugate–gradient method, which is implemented in the Shanno and Phua's (1980) CONMIN algorithm. When dealing with the well-conditioned problem, the conjugate gradient method provides fast functional reduction within the first few iterations. For linear dynamics, its convergence should be achieved in at most M iterations, where M is the number of the control variables. In fact, the rate of convergence depends to a large extent on the quality of the observations. Noisy observations poorly reflect the model dynamics, so the conjugate gradient method will converge slowly and all M iterations will be needed to obtain the required accuracy.

3. The variational optimal control technique applied to a simulated current field

The minimum of the cost function generally is not expected to be equal to zero. The observations have errors and the model is ideal, so the solution is not exactly compatible with the observations. In a partic-
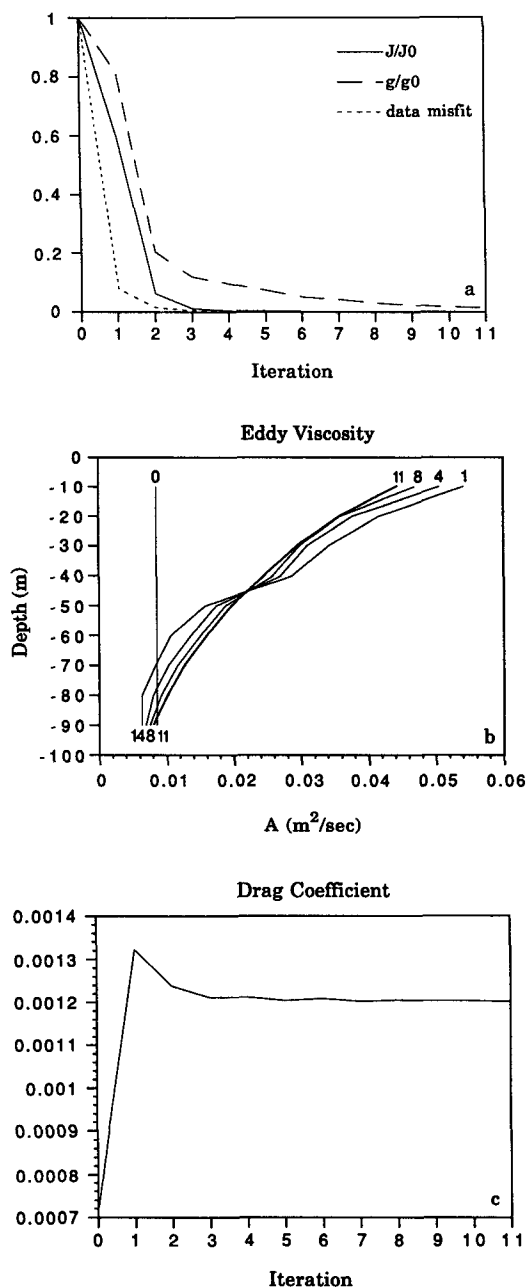

FIG. 1. Diagram for the vertical structure of the numerical model.

FIG. 3. Results from the identical twin experiment. (a) The variation of the cost function J/J_0, the norm of the gradient $|g|/|g_0|$, and the data misfit $(w - \hat{w})^2$ with the number of iterations (scaled by their own initial values); (b) The variation of the eddy viscosity profile during the iterative process (the number denotes the iterations); and (c) The variation of the drag coefficient with the number of iterations.

experiments. In this section, an identical twin experiment is discussed.

The current "observations" in this experiment are obtained by running the original dynamic model forward, using a sinusoidal wind pattern $w = 10 \sin(2\pi t/ T_0)$ (m s^{-1}), where $T_0 = 10$ h. The wind stress coefficient is set to 1.2×10^{-3} (unscaled), and the eddy viscosity profile is shown in Fig. 2. The initial state of the system is at rest.

The model parameters in the dimensional form are chosen as

$$\Delta z = 10 \text{ m}$$
$$\Delta t = 30 \text{ min}$$
$$f = 10^{-4} \text{ s}^{-1}$$

total model integration
time T $= 10$ days
data extension
depth H $= -100$ m
$$\rho_a = 1.2 \text{ kg m}^{-3}$$
$$\rho_w = 1.025 \times 10^3 \text{ kg m}^{-3}$$
$$S_a = 5.0 \times 10^{-2} \text{ m}^2 \text{ s}^{-1}$$
$$S_c = 1.2 \times 10^{-3}$$
$$U_a = 10 \text{ m s}^{-1}.$$

ular case where a simulated field is used, the exact consistency between the "observations" and the model dynamics will make the optimal value of the cost function vanish. The model solution is therefore expected to completely satisfy the characteristics of the "observed" field in these test runs, called identical twin
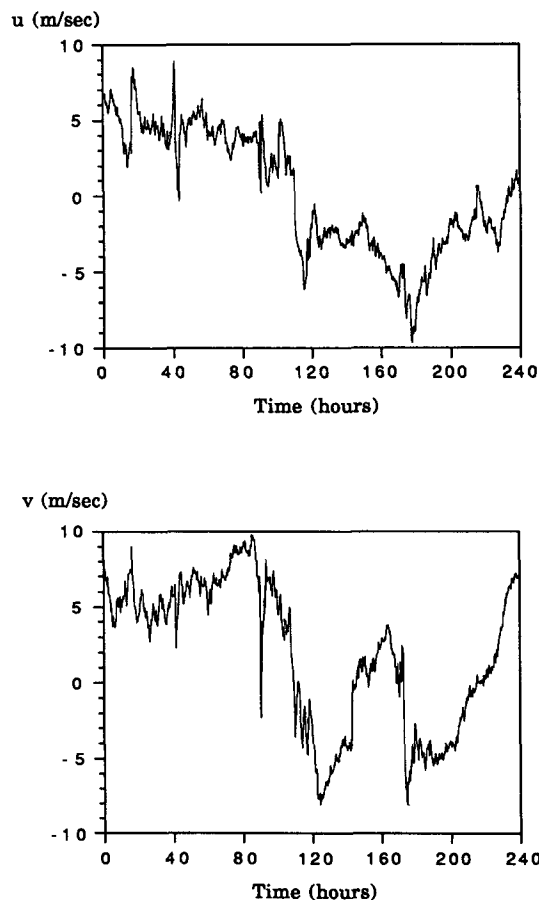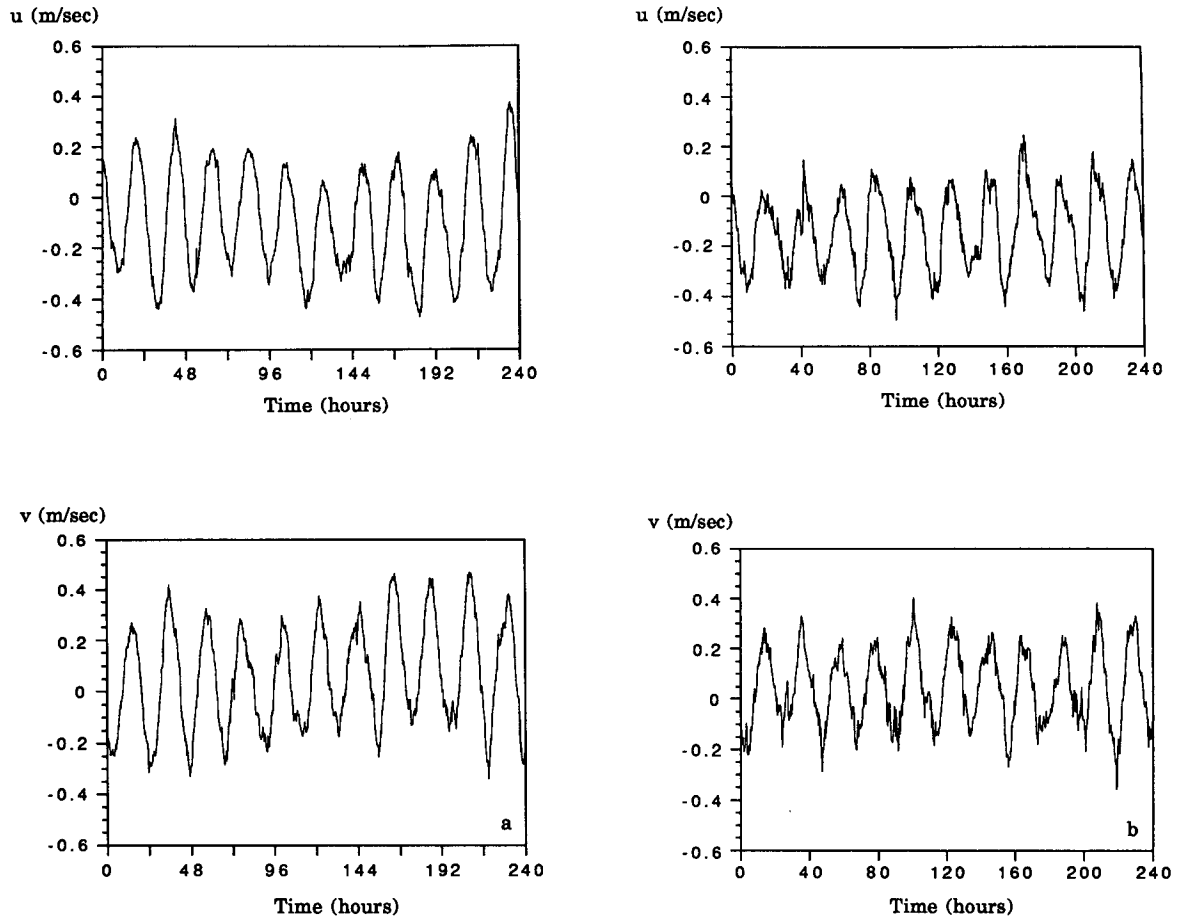

FIG. 4. Time series of wind observations.

FIG. 5. Current observations at (a) 5 m, (b) 25 m, and (c) 50 m.

Both the wind stress parameter and eddy viscosity are treated as unknowns and recovered simultaneously by the optimization process. The initial estimates for A and c_D are given as 0.8×10^{-2} m^2 s^{-1} and 0.72×10^{-3} (unscaled), respectively. Figure 3a shows the values of the cost function, its gradient, and the data misfit versus the number of iterations in the minimization procedure. All values have been normalized by their own initial values to allow a direct comparison of the convergence rate. As can be seen, the cost function drops rapidly in the first couple of iterations. The ratio of the norm of the gradient $|g|/|g_0|$($|g|$ represents $|\nabla J|$ hereafter) also experiences a sharp decrease in the first two iterations. The convergence criterion is satisfied after 11 iterations. The evolution of the eddy viscosity distribution and the drag coefficient during the optimization are displayed in Figs. 3b–c. There is a sharp increase for the drag coefficient (Fig. 3c) during the first iteration, but it overshoots. Corresponding to this strong forcing, the eddy viscosity in the upper 50 meters has a relatively large value in comparison with its true solution (Fig. 3b). This is partly because the current field generated with the chosen initial estima-

tions for the control parameters, which are smaller than their true values, produces a large data misfit in the first iteration. The Lagrange multipliers computed from the adjoint model, are being driven by this big data misfit, and therefore, have a great effect on the calculation of the gradient of the cost function. Hence, a strong correction is made to the previous estimates. The drag coefficient tends towards its true solution after the first iteration and the eddy viscosity is also adjusted gradually. The bold line in Fig. 3b is the converged solution. It shows a very good approximation to its true value (see Fig. 2).

This experiment indicates that the variational adjoint method makes it possible to determine the model unknown parameter and the forcing parameter simultaneously. The wind forcing term is updated at each iteration because of the variation of the wind stress drag coefficient. Its new evolution gives a new model state, which determines the closeness of the model data to the observation. This controls the information the Lagrange multiplier carries, which in turn has a great influence on the new estimate for the wind stress drag coefficient and the eddy viscosity distribution. The al-
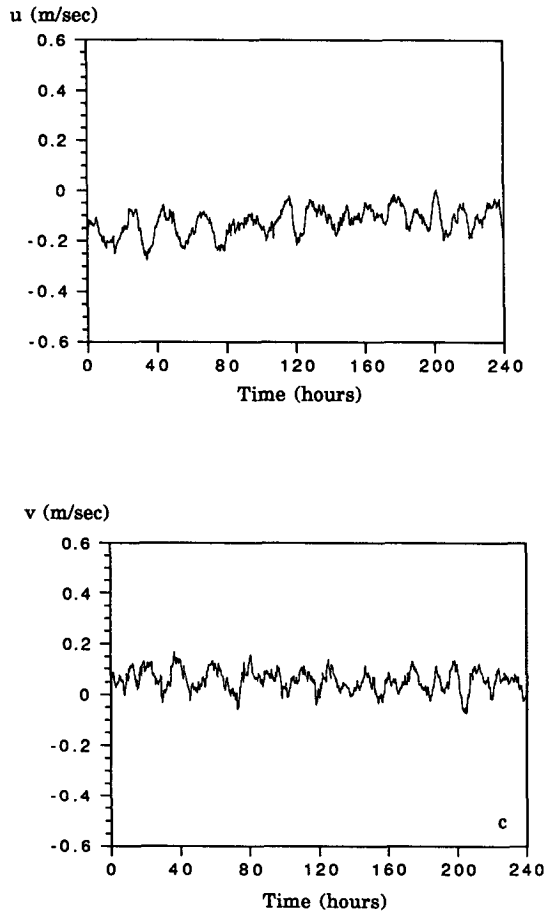
u (m/sec)

v (m/sec)

FIG. 5. (Continued)

LOTUS-3 buoy by WHOI (Tarbell et al. 1984; Bowers et al. 1986). This deployment was located in the northwestern Sargasso Sea (34°N, 70°W) during the summer of 1982. In situ current measurements were made by Vector Measuring Current Meters (VMCMs) fixed at depths of 5, 10, 15, 20, 25, 35, 50, 65, 75, and
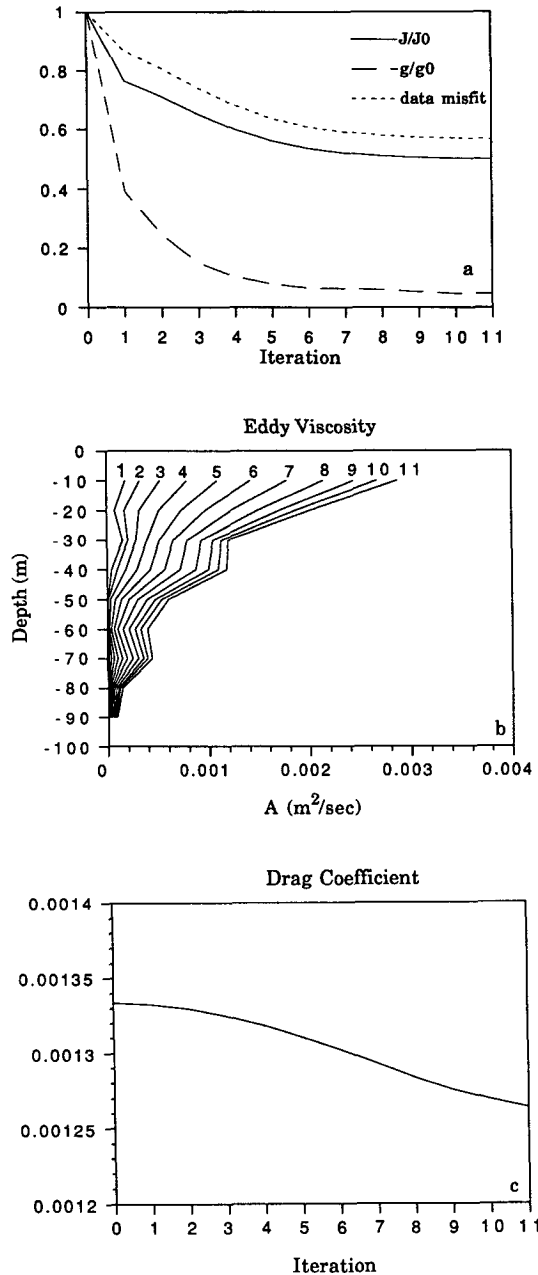

Eddy Viscosity

Drag Coefficient

FIG. 6. Real data assimilation. (a) The variation of the cost function J/J_0, the norm of the gradient $|g|/|g_0|$, and the data misfit $(w - \hat{w})^2$ with the number of iterations (scaled by their own initial values); (b) The variation of the eddy viscosity profile during the iterative process (the number denotes the iterations); and (c) The variation of the drag coefficient with the number of iterations.

gorithm permits the boundary condition and model to adjust simultaneously and approach the best model-data fit efficiently.

It is important to note that the choice of the initial values for the control parameters is arbitrary; however, the solution is independent of the initial guess. But as discussed in section 2.b, for the efficiency of the optimization process, the parameters' initial guess should be as reasonable as possible. For this reason, prior knowledge of the physical background (i.e., the air-sea condition, the oceanic instability, etc.) is desired to help to obtain a good choice.

This experiment has been restricted to an identical twin run, i.e., the "observations" are results from the model without noise. In the following section, we will apply this technique to a real, observed current field.

4. The variational optimal control technique applied to an observed field

a. Data

The oceanographic and meterological field observations used for our analysis were acquired from the
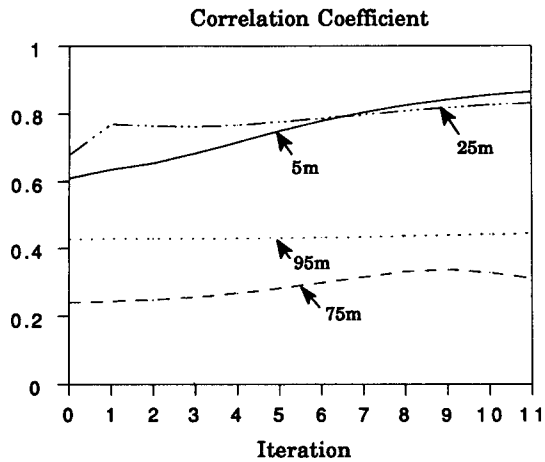
Correlation Coefficient

FIG. 7. The variation of the correlation coefficient at different depths with the number of iterations.

100 meters. The wind speeds were measured by the Vector-Averaging Wind Recorder (VAWR) which was mounted on the tower of LOTUS-3. The sample interval was 15 minutes. These data were kindly supplied by Briscoe, Price, and Weller from WHOI.

Ten days of data were chosen, from 30 June to 9 July 1982. The time series measurements of wind speed are plotted in Fig. 4. The current observations at 5, 25, and 50 m are shown in Figs. 5a–c. Inertial oscillations are dominant at 5 and 25 m. At 50 m the inertial signal is evident but obviously it is incoherent with the motion in the upper layer. This inconsistency is, perhaps, due to other physical phenomena (e.g., diurnal tides, internal waves) or the observation errors.

The measured currents contain the pressure-driven currents (e.g., tides, geostrophic motions) in addition to the locally wind-driven currents. The mean wind-driven current has an amplitude of about 0.05 m s^{-1}, while the pressure-driven current has a root-mean-square value about five times larger (Price et al. 1987). Because we have observations at only one station, it is impossible to compute the pressure-driven motions from the observations. Considering that the time scale of geostrophic motion is much longer than the period of inertial oscillations, we process the data at each depth by removing its trend to filter out the geostrophic components.

Our numerical model has equally spaced grid points in the vertical, but the data are not available at some depths. Linear interpolation is used to fill the gaps.
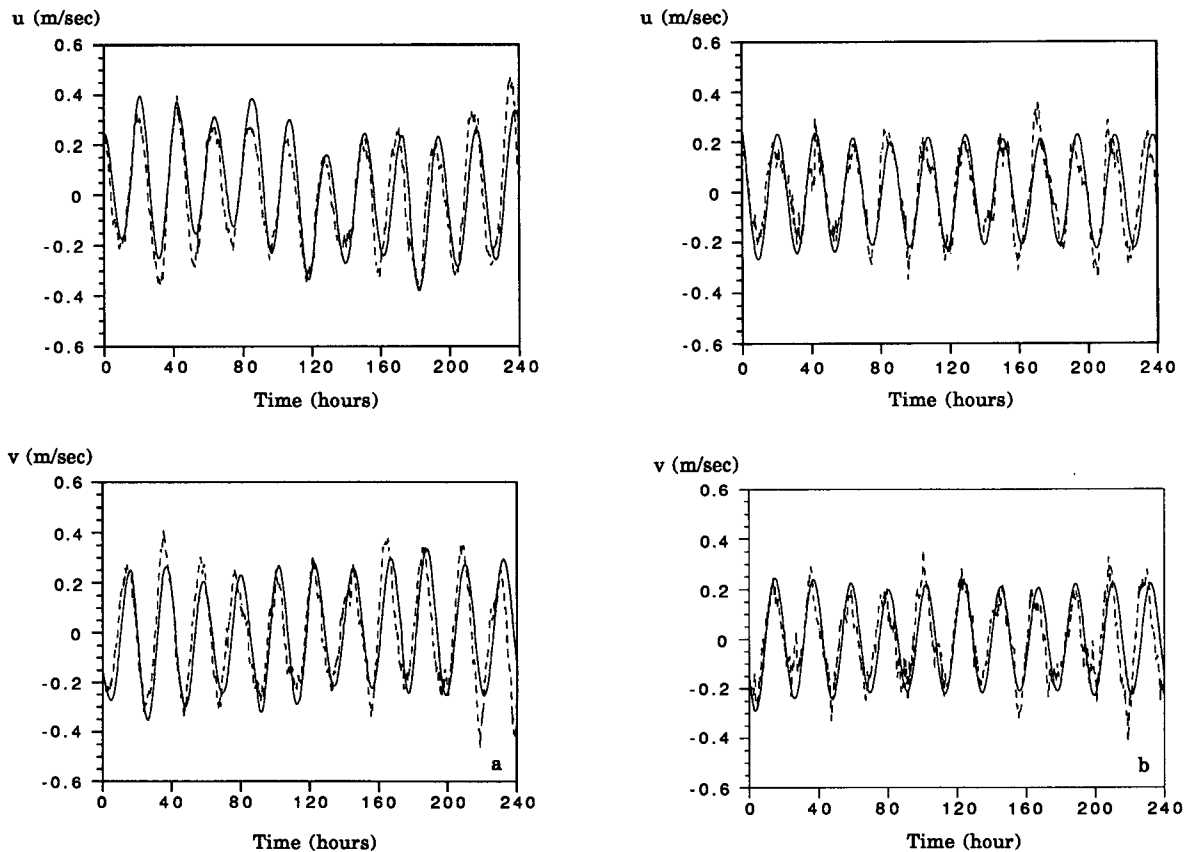

FIG. 8. Comparisons of the modeled (solid) and observed (dashed) current velocities at (a) 5 m, (b) 25 m, (c) 35 m, and (d) 75 m.

However, in principle, additional data is not needed at grid points where there are no measurements.

b. Results

The observed field at starting time (30 June 1982) is taken as the initial model state. Initial guesses for A and c_D are 0.01×10^{-3} m^2 s^{-1} and 1.34×10^{-3}. The model is integrated for 10 days with a time step of 15 minutes, the same as the sample interval.

The variation of the cost function, the norm of the gradient, and the data misfit with the number of iterations are plotted in Fig. 6a. The cost function decreases to about 53% of its initial value after 11 iterations. The norm of the gradient has a rapid reduction during the first few iterations. After 11 iterations, it drops to 5% of its initial value and reaches a steady state. The eddy viscosity profile (Fig. 6b) has a maximum value of 2.9 $\times 10^{-3}$ m^2 s^{-1} at the surface and decreases with depth at iteration 11. The drag coefficient (Fig. 6c) is adjusted gradually and finally reaches 1.26×10^{-3}. Price et al. (1987) inferred an effective viscosity $A = 6.0 \times 10^{-3}$ m^2 s^{-1} by separating the wind-driven current from the

measured LOTUS-3 current and averaging over the whole period. Our results are reasonably consistent with those of Price et al.

The seasonal thermocline is between 20 to 50 meters during this period (Tarbell et al. 1984; Bowers et al. 1986). Figure 6b shows that the eddy viscosity decreases greatly within these depths. This is because the stratification suppresses the turbulent mixing in the thermocline, so the degree of the turbulence, and therefore the eddy viscosity, is much smaller than in the mixed surface layer. Obviously, the physical effects of the stratification are represented in the eddy viscosity profile.

Consider the correlation coefficient that is defined as

$$r = \frac{\sum\limits_{t} qq'}{\left(\sum\limits_{t} q^2 \sum\limits_{t} q'^2 \right)^{1/2}}$$

where q and q' are the model results and the observations, respectively. The mean values have been re-
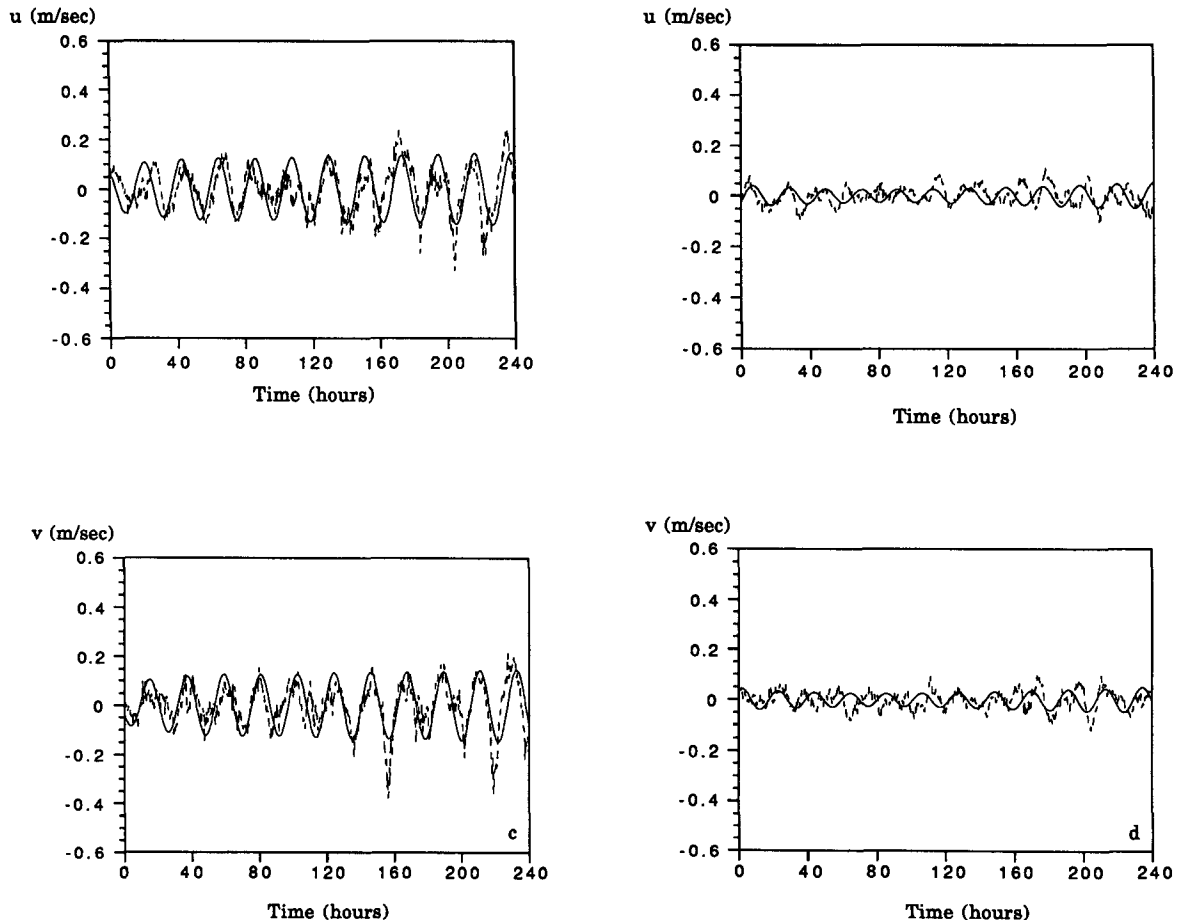

FIG. 8. (Continued)

moved from q and q'. The correlation coefficient defined here represents the degree of fit between the observation and the model counterpart at the same depth. Figure 7 is a plot of the correlation coefficient as a function of iterations at depths 5, 25, 75, and 95 m. It shows that the correlation coefficient has an increase at all these depths with the largest at 5 m and the smallest at 95 m; at 75 m it has the lowest value. This can be understood because the motions in the upper 50m are dominated by inertial oscillations. Below this level, other dynamical processes and the observational errors are superimposed on weak inertial oscillations to make the observed current fields complicated. Our linear dynamical system successfully reproduces the motions in the upper 50 m, but is only able to describe a portion of the motions below 50 m due to the noisy data. The comparisons of the time series of the modeled and observed current fields are displayed in Figs. 8a–d. Obviously, there is very good agreement between model results and observations at 5 and 25 m. At 35 m, although the amplitudes of the modeled current speeds agree with those of the observations, the phases are shifted. However, erratic changes of amplitude and phase of the observations at 75 m are not reproduced by the simple dynamic model. Undoubtedly, most of the residual data misfits (Fig. 6c) come from the lower 50 meters. Since both the cost function and its gradient have a big decrease during the iterative process and reach a steady state after 11 iterations and the estimates of A and c_D improve the model results, we conclude that the solutions of A and c_D at iteration 11 are the best ones derived from these observations.

5. Discussion and summary

We have demonstrated the utility of a variational optimal control technique to assimilate real observations from LOTUS-3 records. The wind stress represents the upper boundary condition in our model and enters in the model equation as a forcing term in the numerical formalism. The variational analysis allows all the dynamics, boundary conditions, and observations to influence the model solution and thus, provides a flexible approach to combining the model results with the observations. By doing so, the wind-stress drag coefficient and eddy viscosity profile have been determined simultaneously and the optimal estimates of the model fields have been obtained as well.

The optimal current field generated successfully reproduces the observed fields in upper 50m, while they are only able to describe part of the motion below 50m due to the inconsistency between model dynamics and data. Actually, no model can fully describe all phenomena occurring in the ocean. The observed data can always be divided into three parts: those that are consistent with the model dynamics, those that are inconsistent with the model dynamics, and those that are due to the observation errors. It is evident that the important characteristics of the variational optimal control method are that it is capable of extracting from the available observations that part which is consistent with the model dynamics and adjusting the final model state to the intrinsic dynamics.

Our dynamic model is a very simple modified Ekman model. The optimal control procedure was used to determine eleven unknown model parameters. All of these parameters are located in the vertical direction of a horizontal station. The advantage of this research is that we have a long, continuous record of measurements with a small sample interval of 15 minutes. We choose this 10-day period because we expected that the data and the model dynamics were basically compatible (i.e., at least in the upper layer where the inertial motions are dominant). The length of the time-series data ensures that the estimated parameters represent the time-averaged values. The small time interval of the measurements greatly improves the accuracy of the estimated parameters since the dominant motion is contained in the high frequency inertial oscillations. The time-mean values of the parameters are the effective values during the chosen period. We expect that these values will be slightly different if the length of the data assimilation is changed.

The variational optimal control is conceptually simple and internally consistent. The adjoint model introduced makes the computation of the gradient of the cost function more efficient than the direct perturbation method does. It is clear that the systematic and quantitative approach that the variational optimal control technique provides can be utilized for a wide variety of problems. It can adjust not only the initial conditions of the model but also the lateral boundary conditions (Le Dimet and Nouailler 1985), as in the case of a limited area model, the upper boundary conditions such as the surface forcing by momentum and heat fluxes, as well as the various physical and numerical parameters that enter the definition of the model.

REFERENCES

Bowers, C. M., J. F. Price, R. A. Weller and M. G. Briscoe, 1986: Data tabulations and analysis of diurnal sea surface temperature variability observed at LOTUS. Woods Hole Oceanographic Institution Tech. Rep., WHOI-86-5, 51 pp.

Carrera, J., and S. P. Neuman, 1986: Estimation of aquifer parameters under transient and steady conditions: 2. Uniqueness, stability, and solution algorithms. *Water Resour. Res.,* **22,** 211–227.

Derber, J. C., 1985: The variational four-dimensional assimilation of analyses using filtered models as constraints. Ph.D. dissertation, University of Wisconsin, Madison, 142 pp.

Gill, P. E., W. Murray and M. H. Wright, 1981: *Practical Optimization.* Springer-Verlag, 377 pp.

Le Dimet, F., and A. Nouailler, 1985: Assimilation of dynamical data in a limited area model. *Variational Methods in Geosciences,* Y. Sasaki, Ed., Elsevier, 181–185.

——, and O. Talagrand, 1986: Variational algorithms for analysis and assimilation of meteorological observations: theoretical aspects. *Tellus,* **38A,** 97–110.

Long, R. B., and W. C. Thacker, 1989: Data assimilation into a numerical equatorial ocean model. II: Assimilation experiments. *Dyn. Atmos. Oceans,* **13,** 413–439.

Luenberger, D. C., 1984: *Linear and Nonlinear Programming.* Addison-Wesley, 491 pp.

Navon, I. M., and D. Legler, 1987: Conjugate–gradient methods for large-scale minimization in meteorology. *Mon. Wea. Rev.,* **115,** 1479–1502.

O'Brien, J. J., 1986: The diffusive problem. *Advanced Physical Oceanographic Numerical Modelling,* J. J. O'Brien, Ed., D. Reidel, 127–144.

Panchang, V. G., and J. J. O'Brien, 1988: On the determination of hydraulic model parameters using the adjoint state formulation. *Modeling Marine System,* I, CRC Press, 5–18.

Price, J. F., R. A. Weller and R. R. Schudlich, 1987: Wind-driven ocean currents and Ekman transport. *Science,* **238,** 1534–1538.

Sasaki, Y., 1970: Some basic formations in numerical variational analysis. *Mon. Wea. Rev.,* **98,** 875–883.

Shanno, D. F., and K. H. Phua, 1980: Remarks on algorithm 500—a variable method subroutine for unconstrained nonlinear minimization. *ACM Trans. on Math. Software,* **6,** 618–622.

Sheinbaum, J., and D. L. T. Anderson, 1990: Variational assimilation of XBT data. Part I. *J. Phys. Oceanogr.,* **20,** 672–688.

Smedstad, O. M., and J. J. O'Brien, 1991: Variational data assimilation and parameter estimation in an equatorial Pacific Ocean model. *Progress in Oceanography,* Vol. 26, Pergamon, 179–241.

Talagrand, O., and P. Courtier, 1987: Variational assimilation of meteorological observations with the adjoint vorticity equation. Part I: Theory. *Quart. J. Roy. Meteorol. Soc.,* **113,** 1311–1328.

Tarbell, S. A., N. J. Pennington and M. G. Briscoe, 1984: A compilation of moored current meter and wind recorder data. Volume XXXV, Long-Term Upper Ocean Study (LOTUS) (Moorings 764, 765, 766, 767, 770), May 1982–April 1983. Woods Hole Oceanographic Institution Tech. Rep., WHOI-84-36, 154 pp.

Thacker, W. C., 1988: Fitting models to inadequate data by enforcing spatial and temporal smoothness. *J. Geophys. Res.,* **93,** 10 655–10 665.

——, and R. B. Long, 1988: Fitting dynamics to data. *J. Geophys. Res.,* **93,** 1227–1240.

Wunsch, C., 1987: Using transient tracers: the regularization problem. *Tellus,* **39B,** 477–492.

——, 1988: Transient tracers as a problem in control theory. *J. Geophys. Res.,* **93,** 8099–9110.